Heliyon 10 (2024) e23421

Contents lists available at ScienceDirect

Heliyon

journal homepage: www.cell.com/heliyon

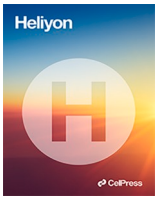

Fabrication and performance analysis of keratin based-graphene oxide nanocomposite to remove dye from tannery wastewater

Shazneen Chowdhury [a], Md Elias Uddin [a,*], Md Ashikur Rahaman Noyon [a], Md Mahmudul Hassan Mondol [b], Ibrahim M. Maafa [c], Ayman Yousef [c,d]

[a] Department of Leather Engineering, Faculty of Mechanical Engineering, Khulna University of Engineering & Technology, Khulna 9203, Bangladesh
[b] Department of Chemical Engineering, Faculty of Mechanical Engineering, Khulna University of Engineering & Technology, Khulna 9203, Bangladesh
[c] Department of Chemical Engineering, Faculty of Engineering, Jazan University, Jazan 11451, Saudi Arabia
[d] Department of Mathematics and Physics Engineering, Faculty of Engineering at Mataria, Helwan University, Cairo 11718, Egypt

ARTICLE INFO

Keywords:
Adsorption
Graphene oxide
Keratin
Nanocomposite
Wastewater

ABSTRACT

In recent years, nanomaterials and composites have become increasingly significant as adsorbents in the removal of dyes and phenolic contaminants from wastewater. This study presents the development and application of a keratin-based graphene oxide nanocomposite, distinguished by its enhanced biocompatibility, cost-effectiveness, and strong affinity for organic compounds, making it highly effective in reducing dyes within tannery effluent. The nanocomposite was prepared via solution casting method, with dispersibility, chemical bonding, and morphology analyzed by UV–Vis spectroscopy, FTIR, and SEM, respectively. Furthermore, investigations of the influence of several factors, such as contact time, pH, and adsorbent dosage on the optimization of the process were conducted. An observation indicated a reduction of approximately 98.8 % in dye content within 20 min, achieved through the use of an adsorbent dosage of 1.5 g/L, with the solution pH maintained at 5. Subsequently, adsorption kinetics and isotherm modelling were analyzed. The results revealed that the adsorption process follows the pseudo-second-order kinetics and Freundlich isotherm models. Hence, the adsorption could be explained as chemisorption with a multilayer adsorption mechanism. Notably, a substantial reduction in parameters such as Biological Oxygen Demand (BOD) and Chemical Oxygen Demand (COD) was also achieved up to 62 % and 79 %, respectively. Therefore, the developed adsorbent could be suggested as a viable candidate for eliminating dyes from the wastewater, especially from the tannery effluent.

1. Introduction

In today's world, water pollution is a significant issue. Aromatic dyes from industries like textiles, leather, paper, food, and cosmetics contribute to this problem in our aquatic ecosystems. These appreciated substances have become menacing pollutants, threatening aquatic life and human well-being [1–3]. The global production of dyes has increased, exceeding 8 million tons annually, leading to the indiscriminate release of effluents that imperil both aquatic and terrestrial ecosystems [4]. The leather industry uses a lot

* Corresponding author.
E-mail address: eliasuddin@le.kuet.ac.bd (M.E. Uddin).

https://doi.org/10.1016/j.heliyon.2023.e23421
Received 15 October 2023; Received in revised form 20 November 2023; Accepted 4 December 2023
Available online 12 December 2023

of dyes to improve the quality and chemical properties during the wet finishing process. Unfortunately, a significant portion, ranging from 10 % to 50 %, is often lost during the subsequent dye washing procedures. Many of these dyes elude conventional wastewater treatment methods, persisting in the environment [5]. These recalcitrant dyes pose various health risks in humans, including hemolysis, hypertension, jaundice, organ damage, tissue necrosis, and respiratory disorders [6]. The discharge of tannery wastewater poses a significant environmental threat due to its impact on parameters like Biological Oxygen Demand (BOD) and Chemical Oxygen Demand (COD). Tannery wastewater typically contains organic compounds and chemicals used in leather processing, which contribute to high BOD and COD levels. When this wastewater enters natural water bodies, it consumes oxygen as microorganisms break down the organic matter, leading to decreased oxygen availability for aquatic life. This reduction in oxygen levels, known as oxygen depletion, can result in the death of fish and other aquatic organisms, disrupting the delicate balance of ecosystems and causing long-term environmental damage [2–4]. Effective treatment of tannery wastewater is crucial to mitigate these detrimental effects and protect the environment [3,5]. Highly stable aromatic structures of dyes render them resistant to natural degradation. Furthermore, the discharge of such turbid effluents blocks sunlight penetration, diminishing photosynthesis in aquatic ecosystems, ultimately disrupting food chains, reducing productivity, and impairing gill function [7,8]. Consequently, the imperative for an effective wastewater treatment system to counteract this anthropogenic menace is undeniable.

Traditionally, wastewater treatment plants in the leather industry have relied on physico-chemical and biological processes for example, flocculation, sedimentation, and activated sludge [9]. However, this approach is marred by issues such as secondary contamination from synthetic chemicals in treated water and the impracticality of large-scale application due to the cumbersome sludge management and added operational expenses [10]. Hence, there is an urgent requirement for research focused on sustainable approach for treating dye wastewater. In this context, adsorption has been considered as one of the most favored remediation techniques for pollutant dye removal due to its simplicity, cost-effectiveness, ease of implementation, and adaptability [11]. When it comes to the adsorptive removal of organic contaminants from water, carbon-based nanomaterials, including porous carbon, charcoal, fullerenes, carbon nanotubes, and graphene, have gained substantial traction [12–21]. These materials are prized for their affordability, expansive surface area, ease of modification, and strong affinity for environmental pollutants [12]. Among these, graphene has emerged as a frontrunner in the realm of adsorbents for water purification, boasting unique physicochemical properties such as an expansive specific surface area (2630 m^2/g), mechanical flexibility, thermal stability, and chemical resilience [13]. Within graphene family, graphene oxide (GO), an extensively oxidized form of graphene, presents numerous oxygen-containing groups, including epoxy and hydroxyl groups on the basal plane and carboxylic groups at the sheet's edges [14]. It's worth noting that one challenge with GO is the prevention of aggregation on its nanosheets to maintain electrostatic repulsion. In contrast, GO-based composite adsorbents offer distinct advantages over traditional adsorbents, including reusability and biocompatibility [15]. Therefore, researchers have explored the grafting of bio-composite materials like chitosan, cellulose, and keratin with GO to augment surface area for adsorption and prevent nanomaterial aggregation into graphite. This strategy holds promise for enhancing adsorption performance and biocompatibility, as demonstrated in the creation of hydrogels for the removal of emerging pollutants like ciprofloxacin [16]. Surprisingly, there has been limited exploration of the GO-K nanocomposite's potential for removing leather dyes from tannery wastewater. While some studies have reported impressive reductions in turbidity from raw surface water using GO coagulants [17], others have investigated GO adsorption for recovering efficacy from textile effluents [18]. Previously GO-FO and GO-K-CS nanocomposites were fabricated to remove turbidity from tannery wastewater [19,20]. A nanocomposite consisting of activated carbon supported ZnO/ZnWO4 was employed to investigate the kinetics of the photocatalytic mineralization of oxytetracycline and ampicillin in simulated wastewater [21]. In contrast, Silk Fibroin (SK)-keratin adsorbents have been lauded for their ability to achieve removal efficiencies as high as 95.3 % for Reactive Black 5 (RB5) [22].

Additionally, there is a suitable biomaterial known as keratin (K), the most abundant non-food protein, used to separate various contaminants from wastewater, including organic and inorganic substances, oil, fat, heavy metals, and so on [20]. Keratin is a ubiquitous, renewable natural polymer sourced from waste materials such as chicken feathers, wool, and hair discarded by slaughterhouses and leather industries, accounting for millions of tons annually [23]. While keratin poses challenges due to its high sulfur content and self-extinguishing properties, necessitating innovative disposal solutions, it features numerous amino groups, carboxyl groups, and other functional groups that can serve as effective dye adsorption sites [24]. Despite the need to break disulfide links and disrupt its molecular structure during extraction, compromising its mechanical properties and reusability, extensive efforts have been directed towards enhancing the mechanical characteristics of keratin (K)-based materials [23,24]. Graphene oxide (GO) nanoparticles, known for their enhanced mechanical strength and increased surface area, present a potential solution to enhance the effectiveness of keratin during the fabrication of composites.

This study unveils a groundbreaking approach to address the adsorption of three anionic dyes found in tannery wastewater through the application of the GO-K nanocomposite. In contrast to activated carbon, the investigated adsorbent demonstrated exceptional efficacy in the removal of anionic dyes, specifically Acid Orange II, Direct Orange 2 GL, and Acid Red 27. Notably, GO-K exhibited a remarkably high efficiency, achieving a 98.8 % removal of dye from tannery wastewater within just 20 min, surpassing outcomes observed in previous studies. This heightened performance underscores the superior capabilities of the GO-K nanocomposite, signaling its potential for widespread applications in treating turbid dye wastewater. The underlying mechanism governing effective dye adsorption is attributed to chemisorption, further emphasizing the innovative nature of this research. Future investigations should focus on assessing the reusability of the fabricated nanocomposite adsorbent to validate its commercial feasibility and cost-effectiveness.

2. Materials and methods

2.1. Wastewater collection and pre-treatment

Wastewater, an inherent by-product of the intricate leather wet finishing process, was meticulously collected from a local leather manufacturing industry. They were kept within durable plastic containers, not once but on three distinct occasions, ensuring a robust dataset. The wastewater composed of unveiled-Anionic dyes, including the Acid Orange II, the Direct Orange 2 GL, and the Acid Red 27, were unequivocally traced as the key constituents of the collected effluent. Therefore, these three dyes were most definitely present in the collected effluent [25,26]. Before delving into nanocomposite adsorption, sedimentation was initially employed as the prelude, providing access to an optimized supernatant for subsequent physiochemical analyses. Here, the focal point of our endeavor was the reduction of dye molecules, a pivotal metric that held our unwavering attention. A parallel exploration was embarked for evaluating the essence of the wastewater meticulously both before and after treatment. The Biochemical Oxygen Demand (BOD) of wastewater was determined following APHA Standard Methods (5210 B). The initial dissolved oxygen of the collected was measured, with subsequent dilution performed when necessary. BOD bottles were inoculated with seed water, and the sample was added, ensuring appropriate dilution. The bottles were sealed and incubated at 20 ± 1 °C for five days. The final dissolved oxygen was measured, and BOD was calculated using the formula:

$$BOD = \frac{Initial\ DO - Final\ DO}{P} \times Dilution\ Factor$$

Here P represents the proportion of the sample volume to the total volume of the BOD bottle. The resulting BOD value, reported in mg/L, was obtained through the completion of the procedure. Specific details and requirements were followed according to the APHA Standard Methods. The BOD of the wastewater after treating with adsorbent was also measured following the same process. The Chemical Oxygen Demand (COD) of wastewater was determined in accordance with APHA Standard Methods (5220C). The collected sample was digested with a strong oxidizing agent, potassium dichromate, in the presence of sulfuric acid. The excess dichromate was titrated against ferrous ammonium sulfate, and the amount of oxygen required for oxidation was quantified. The COD results, expressed in milligrams of oxygen per liter (mg/L), were obtained after completing the titration. Specific details and requirements outlined in the APHA Standard Methods were adhered to throughout the procedure.

2.2. Chemical reagents

All chemicals utilized in the experiments were of analytical grade and sourced from Sigma Aldrich Bangladesh Ltd. Through a local supplier in Khulna. Specifically, the crystalline graphite flakes were exploited for GO synthesis, and the graphite flakes were oxidized using a combination of sulfuric acid (H_2SO_4), hydrogen peroxide (H_2O_2), and potassium permanganate ($KMnO_4$). To regulate the pH, sodium hydroxide (NaOH) and hydrochloric acid (HCl) were used. The unhairing of goat skin involved the application of lime, sodium sulfate (Na_2S), and wetting agent (LD-600). On the other hand, sodium hydroxide (NaOH), Lipex enzyme 100 T (Novo enzymes, Denmark), and proteolytic enzyme (Esperase 6.0 T) were taken into account for keratin extraction. Potassium dichromate ($K_2Cr_2O_7$), Ammonium sulfate, starch, potassium iodide, sodium thiosulfate, silver sulfate, and FAS solution were used to determine pH, BOD, and COD.

2.3. Preparation of GO from natural graphite flakes

Natural graphite flake (crystalline, 300 mesh) was subjected to oxidation to prepare GO using a modified Hummers process [27]. At the beginning, 46 mL of concentrated H_2SO_4 (95 %) was added to 2 g of natural flake graphite in an ice bath (~0–5 °C), and the mixture was continuously stirred for 2 h. After carefully combining 6 g of potassium permanganate, the solution was agitated for 2 h at a temperature below 20 °C. After that, the solution was stirred in an oil bath for an additional 6 h at 35 °C. After certain duration, the mixture changed from black to a light brown paste. Subsequently, 92 mL of de-ionized water was carefully added to the suspension at this juncture, and the mixture was stirred for the next 2 h. After the liquid had cold, 10 mL of 35 wt % H_2O_2 was added to begin the oxidation process and stirred for 2 h. The suspension undergoes another color shift during the process, going from brown to pale yellow. The precipitate was thought to be washed with 5 % HCl to get rid of any remaining metal ions and centrifuged with DI water. Thereafter, GO was rinsed with DI water once more to get rid of the sulfate ions, and washing was maintained until the pH of the solution was neutral. Then, GO was separated by vacuum-assisted drying at 60 °C. Finally, freeze-drying procedure was used in order to collect the detached GO for the following experimental procedures.

2.4. Preparation of keratin powder

Using a traditional unhairing procedure, goat hair was extracted from goat skin that had been collected from a local slaughterhouse in Khulna, Bangladesh (painting by lime, H_2S, and LD-600). Extracted hair was carefully cleaned under running water and dried afterwards in an oven at 70 °C. In this case, keratin removal from sheep wool through weight molecular disintegration was studied [28]. Enzymatic hydrolysis and subsequent alkali hydrolysis were categorized as the two phases of the process. In accordance with a previous study [29], goat hair was minced into tiny snippets prior to hydrolyzation. Next, Lipex enzyme 100 T (Novo enzymes, Denmark)

was used for enzymatic activities, where 1 g of enzyme, 2 L of water, and 100 g of goat hair were combined and left at 40 °C for 24 h. Following that, 2 g of the produced material was hydrolyzed once again for 24 h in 30 mL of 0.1 N NaOH solution. For subsequent processing, the pH of the suspension (pH 9) was adjusted with HCl and 0.5 g of the proteolytic enzyme. Esperase 6.0 T was added to increase the breakdown rate of the keratin. The liquid keratin solution was then heated at 90 °C to deactivate the enzyme after the solid phase and suspension had been separated by filter paper. After that, it was dried in an oven at 60 °C for 48 h by vacuum evaporator. Finally, it was ground into keratin powder.

2.5. Fabrication of GO-K composite

A simple solution mixing procedure was used to synthesize the GO-K nanocomposite [20]. The synthesis process commenced with the creation of a keratin solution, achieved by dissolving 1 g of keratin in 85 mL of glacial acetic acid (75 %), stirred for 3 h at room temperature [30]. These solutions were then combined with different concentrations of graphene oxide (GO) to produce GO-K nanocomposites at 5, 10, 15, 20, and 25 % w/w in the form of GO ethanoic suspensions [18]. To prepare the GO-K combinations (5 %, 10 %, 15 %, 20 %, and 25 %), five GO stock solutions were made by weighing 0.05 g, 0.1 g, 0.15 g, 0.20 g, and 0.25 g. These were suspended in ethanol and sonicated for 25 min at 35 kHz, respectively. The introduction of keratin solutions dropwise into the GO solutions followed, and the mixtures underwent 2 h of sonication to ensure homogeneity. Subsequently, the solutions were transferred to a 100 mL conical flask, refluxed for 24 h at 80 °C, and then cooled to room temperature. After that, the residues were gathered and thoroughly cleaned with DI water to eliminate any unreacted substances. The resulting slurries were heated once again in an oven at 60 °C for approximately 72 h, and the remnants were ground for subsequent experiments. Finally, five nanocomposites containing GO and keratin were fabricated and labeled as GO-K05, GO-K10, GO-K15, GO-K20, and GO-K25. All the five synthesized composites were compared based on their dye removal efficiency against time, and one adsorbent showing maximum % removal of turbid dye in minimum time was selected for further assessment and characterization. The composition is presented in Table 1.

2.6. Characterization of GO-K nanocomposite

The XRD test was conducted using BRUKER's D8 advance machine, which was employed to ascertain the degree of crystallinity. SEM was used to examine the surface morphology of GO-K10 nanocomposite (model: Ultrahigh-Resolution Schottky Scanning Electron Microscope SU8800). Fourier transform infrared spectroscopy (FTIR) analysis confirmed the chemical bonding in that GO-K10 nanocomposite which employed a frequency range of 400–4000 cm^{-1} (model: NICOLET 6800 FTIR equipment, Thermo Scientific, USA). Moreover, the dispensability of the GO-K (GO-K10) in aqueous media at room temperature was analyzed by UV–Vis spectroscopy (model: UVS-2100 SCINCO).

2.7. Batch adsorption analysis

To facilitate the removal of dye molecules, the consideration was given to a batch adsorption process utilizing the GO-K nanocomposite. Performance parameters, including pH, adsorbent dose, and contact time, were systematically evaluated to ensure maximum removal. The studies were carried out at an agitation speed of 150 rpm at 28 °C. Either 0.1 M NaOH or 0.1 M HCl was used to alter the pH of the solution during analysis. Several concentrations of adsorbents, ranging from 0.01 to 0.45 g/50 mL, were added to the solution to study the impact of adsorbent dosages. The effect of reaction time within a 15–60 min window and the effect of pH in the range of 3–9 were both taken into consideration. Finally, the assessment of the efficiency in eliminating dye turbidity from the treated samples was conducted by utilizing a UV–Vis spectrophotometer configured to measure absorbance in the range of 200 nm–800 nm. Equation (1) was applied to determine the percentage of dye removal by the adsorbents.

$$R = \frac{C_o - C_f}{C_o} \times 100\% \quad (1)$$

Where C_o is the dye concentration (mgL^{-1}) before the batch adsorption process, and C_f is the dye concentration (mgL^{-1}) after the batch adsorption process.

Table 1
Composition of GO-K nanocomposites.

Sample	GO Percentage	Keratin Percentage
GO-K05	5	95
GO-K10	10	90
GO-K15	15	85
GO-K20	20	80
GO-K25	25	75

3. Results and discussion

3.1. XRD analysis

To decipher the intricate structure of our nanocomposite, XRD analysis of GO, Keratin, and the fabricated GO-K10 (the best adsorbent -vide infra) nanocomposite, was conducted as illustrated in Fig. 1. The exploration commenced with as-synthesized GO, which exhibited a noticeable broad peak at 2θ (where θ represents the diffraction angle), located approximately at 10.5°. This revealed an interlayer spacing of 0.83 nm. This observation validated the successful oxidation of graphite powder via concentrated acids and $KMnO_4$, leading to the formation of GO. The presence of numerous oxygen-containing functional groups on its surface, coupled with electrostatic repulsion among the negatively charged GO sheets, facilitated the effective dispersion of GO [20]. Conversely, pure keratin powder manifested two characteristic peaks at 12.9° and 22.1°, emblematic of the amorphous nature of keratin. Intriguingly, the combination of GO and Keratin ushered in a fascinating transformation, as evidenced by the emergence of two distinct peaks at 2θ values of around 18.4° and 22.6°, respectively. This shift signified subtle alterations in pure keratin, with observable diffraction peaks reminiscent of graphite oxide, indicating successful exfoliation of GO [31]. This transformation found its roots in the synergistic interplay between the amino and hydroxyl groups within the keratin unit and the polycationic nature of Keratin in acid-rich environments. These factors paved the way for electrostatic attraction and hydrogen bonding between GO and Keratin. This facilitated the homogeneous dispersion of GO and Keratin at molecular scales [19,20]. This, in turn, bolstered interfacial adhesion, enhancing the overall performance of fabricated nanocomposite [19,32]. Furthermore, the nanocomposite exhibited a heightened diffraction intensity compared to pure keratin, reflecting an increased crystalline degree in keratin upon the addition of GO. Interestingly, the chemical structure of keratin within the composite remained relatively unaltered with the introduction of GO, underscoring the existence of a distinctive interaction between GO and Keratin [20].

3.2. SEM analysis

Fig. 2 provides a fascinating insight into the morphological attributes of GO, Keratin, and the transformative GO-K10 nanocomposite, as meticulously examined through SEM analysis. As evident from Fig. 5(a), heightened oxidation and enhanced molecular-level dispersibility were discernible in GO, culminating in a notable reduction in agglomeration [33]. Moving to Fig. 5(b), a remarkable transformation unfolded as the material elongated and thinned along the fiber axis, indicative of substantial changes in the cuticle cells. These alterations were attributed to the influence of stretching conditions and keratin hydrolysis, revealing the dynamic nature of this intricate process. Meanwhile, the surface of the GO-K10 sheets, as depicted in Fig. 5(c), revealed a captivating multilayered structure. This structure is brimming with accessible nanochannels that facilitate the swift traversal of small molecules-a crucial attribute in expediting the separation of water contaminants [19,32]. The surface morphology of the GO-K10 composite after adsorption was shown in Fig. 5(d). In stark contrast to the agglomeration often witnessed in GO, this examination of GO-K10 revealed an integral structure, devoid of such agglomeration. This phenomenon could be attributed to the incorporation of keratin within the GO matrix, which served to diminish GO's inclination toward reaggregation [34]. These subtle structural modifications provide a clear insight into the intricate interactions among the constituents (GO and Keratin) within our nanocomposite, that support its performance.

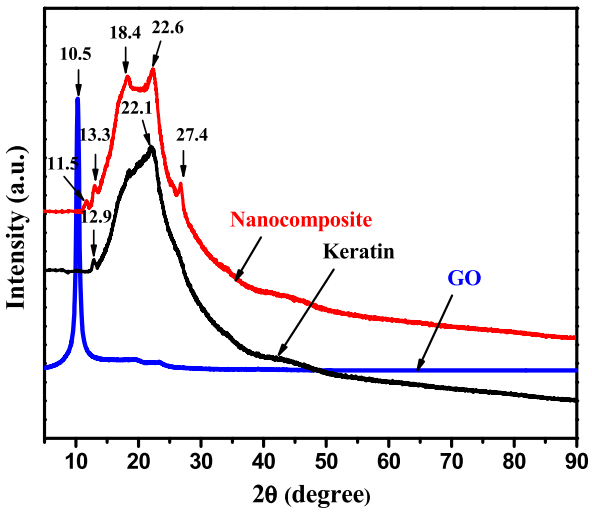

Fig. 1. XRD analysis of pure GO, Keratin, and GO-K10 nanocomposite.

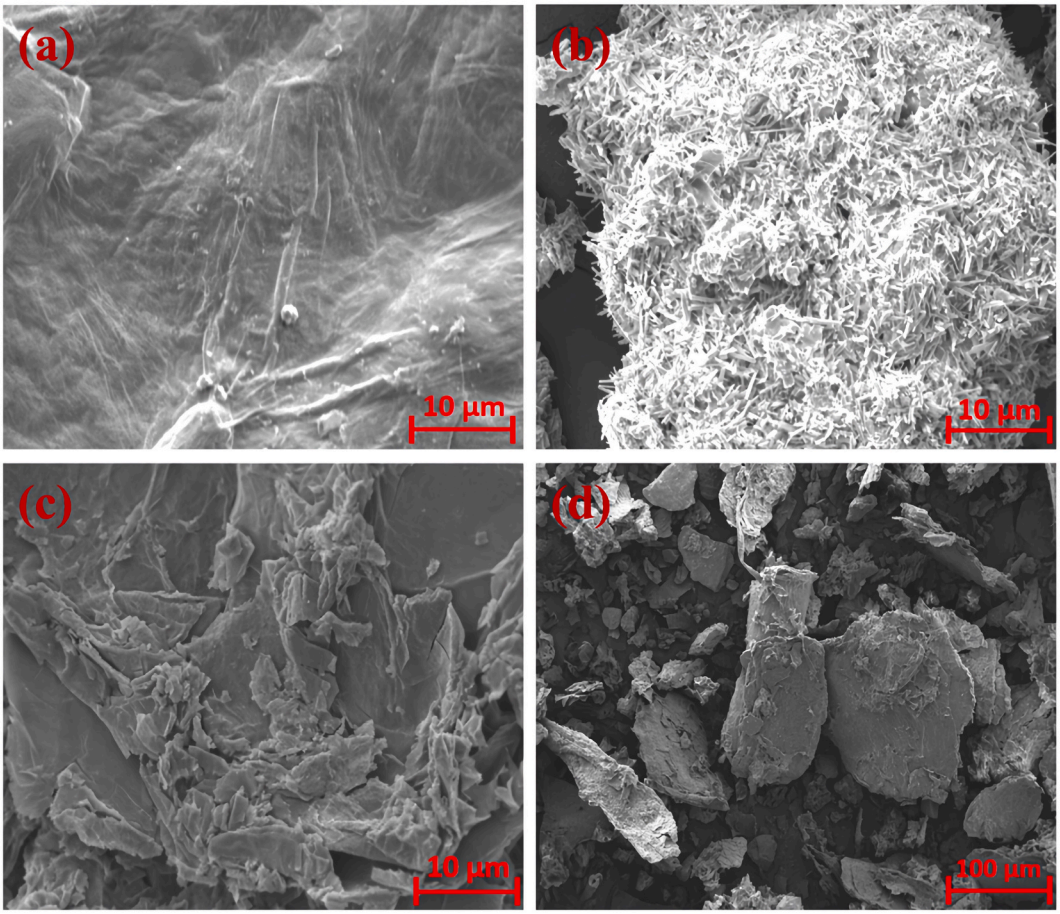

Fig. 2. SEM analysis of (a) pure GO, (b) Keratin, and (c) GO-K10 nanocomposite (before adsorption) (d) GO-K10 nanocomposite (after adsorption).

3.3. FTIR analysis

According to their vibrational patterns in Fig. 3, the FTIR spectra of pure GO, Keratin, and GO-K10 nanocomposite revealed the existence of several oxygenated functional groups. The FTIR spectra of GO revealed a significant peak at 3430 cm^{-1} that identified the

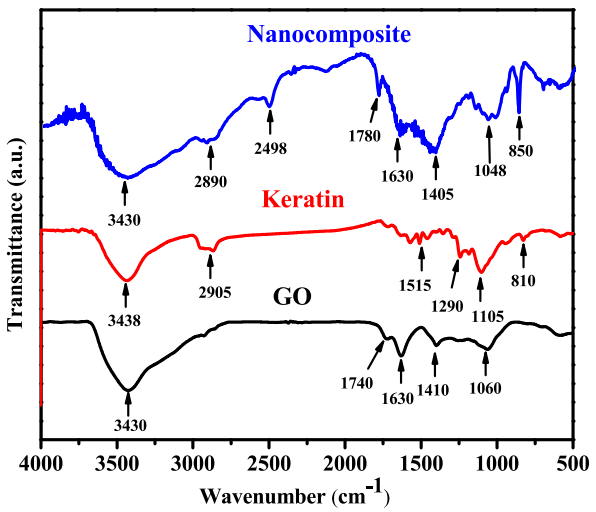

Fig. 3. FT-IR analysis of pure GO, Keratin, and GO-K10 nanocomposite.

O–H stretching of carboxyl functional groups as a result of the restoration of the conjugated aromatic system. The adsorption peak at 1630 cm^{-1} allowed for the identification of carboxyl group presences. In addition, the bands at 1740, 1410, and 1060 cm^{-1} characterized (C═O), corresponding to the stretching of the alkoxy and epoxy functional groups in GO [31]. The FTIR spectra of keratin demonstrated the presence of hydroxyl groups and carboxylic acid groups at wavelengths between 3438 and 2905 cm^{-1}, respectively. The bands of 1515, 1290, and 1105 cm^{-1}, respectively, were used to identify the vibration of the peptide bonds in keratin (Amide I, II, and III). The differentiation between nanocomposite and pure materials primarily stemmed from the presence of distinct spectral peaks related to C–H stretching, C═O bending, and N–H bending in the composite materials. These differences were notably observed at 2890, 2498, 1405, and 1048 cm^{-1} [35]. Consequently, the bonding between the GO and Keratin of the nanocomposite (GO-K) through amide linkages was confirmed, as explained earlier.

3.4. UV–vis spectroscopy analysis

Fig. 4 highlights the UV–Vis spectra of pure GO, Keratin, and GO-K10 nanocomposite, respectively. In the case of GO, a sharp peak around 230 nm is attributed to the C═C π-π* transition, while a narrow band at 300 nm is related to the C═O to n → π* transitions [36,37]. This signal guaranteed the presence of various oxygenated functional groups in GO. Based on the conjugated system with a double bond, the presence of a K band is represented by the UV–Vis absorption spectrum of the keratin band at 265 nm. A connection between peptide bonds and amino acids was confirmed by this revelation [38]. When it comes to nanocomposites, the peak of the π-π* transition changed to 296 nm, indicating the restoration of conjugated structures that can be connected to the complex synthesis of GO and keratin involving hydrogen bonds and electrostatic interactions [39].

3.5. Effects of various parameters

3.5.1. Effect of pH

The solution's pH is a critical factor to be considered during the adsorption process to ensure maximum effectiveness. In this analysis, a solution pH range from 3 to 9 was specifically investigated and represented in Fig. 5. Significant impacts on both the amount of ionization and the surface charge of the adsorbent were observed due to solution pH [40]. The highest removal percentage was achieved under weakly acidic conditions (pH 5.0), while a rapid decrease in removal percentage was observed in slightly to severely alkaline conditions (pH > 5). Dyes, being complex aromatic organic compounds with various functional groups, exhibit varying ionization potentials in response to pH, leading to pH-dependent alterations in the net charge of dye molecules [19,20]. It's noteworthy that the point zero charge (pHPZC) of GO was found to be at pH 7.5, making the adsorption of anionic dye molecules favorable in solutions with pH levels lower than pHPZC, and cationic substances more favorable at higher pH levels than pHPZC [41]. Hence, under weakly acidic conditions (pH 5), a greater adsorption capacity was demonstrated by the GO-based composite. The number of active sites accessible for adsorbing contaminating dye molecules increased when pH levels rise (from 3.0 to 5.0), due to the reduction of hydrogen ions [42]. Conversely, in an alkaline environment, higher concentrations of OH^- ions compete with anionic dyes, leading to a reduction in the percentage of dye removal. Furthermore, flock formation and pollutant settling happened more slowly in an alkaline pH environment, which lowers the percentage of dye removal [16].

3.5.2. Effect of adsorbent dose

An increase in the amount of adsorbent typically results in an augmentation of the accessible surface area. Nonetheless, to avoid both excessive adsorbent use and settling concerns, process optimization becomes imperative. Gradually introducing the adsorbent led

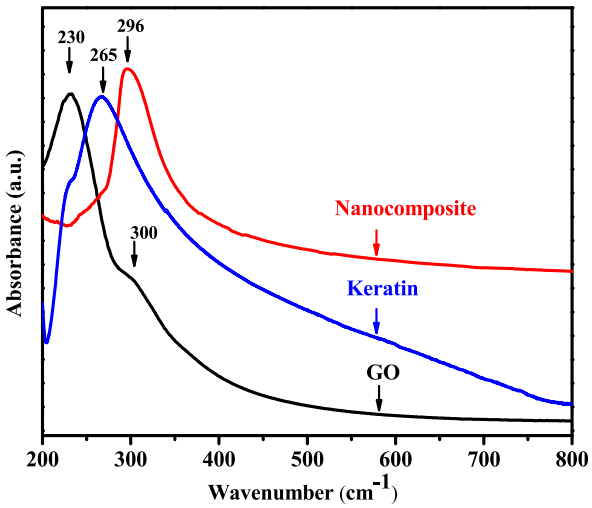

Fig. 4. UV–Vis spectroscopy of pure GO, Keratin, and GO-K10 nanocomposite.

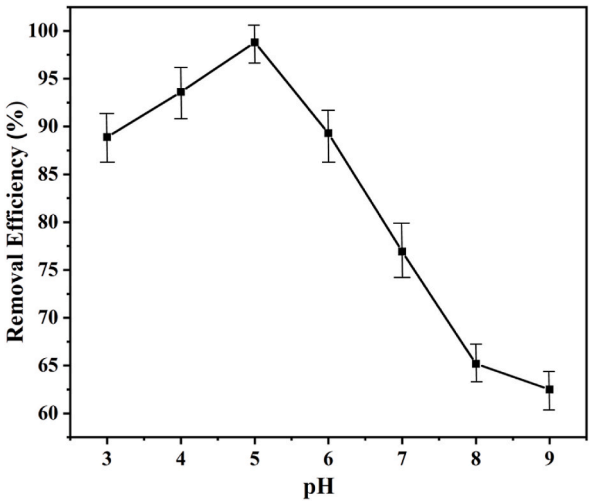

Fig. 5. Effect of pH on dye removal.

to a significant rise in the amount of removed dye, attributable to the proliferation of active binding sites. However, a critical threshold was reached, beyond which the removal rate plateaued, rendering further adsorbent addition ineffectual. This phenomenon became notably apparent at equilibrium, as the abundance of adsorbent binding sites surpassed the concentration of adsorbate [20,40]. This phenomenon is represented in Fig. 6, demonstrating a significant enhancement in removal performance achieved with an adsorbent quantity ranging from 0.1 to 0.45 g. The maximum adsorption capacity was ascertained with 0.15 g of the nanocomposite adsorbent. This optimal quantity was determined by the presence of an ideal number of unoccupied active binding sites. However, beyond the 0.15 g threshold, the performance exhibited a decline with additional adsorbent introduction, primarily attributed to the excessive precipitation of adsorbent or a heightened solid-to-liquid ratio [43].

3.5.3. Effect of contact time

The above illustrated % removal of dye vs reaction time graph in Fig. 7 demonstrates that the adsorption process proceeded in three stages: (i) quick adsorption, (ii) significant decline in adsorption rate and (iii) equilibrium adsorption. In the beginning, the mass transfer of adsorbate molecules to the surface of the adsorbent showed how quickly adsorption occurred. The reduced availability of external active binding sites compared to the first stage can thus be used to explain the declined adsorption capacity. Ultimately, the state of adsorption equilibrium has been attained when the active sites are no longer available for further absorption [20,40]. Active sites of biochar or adsorbent significantly courage the photocatalytic adsorption and degradation/reduction [44]. Several contact times ranging from 10 to 45 min were used in a series of adsorption investigations. According to the results of the analysis of the data in Fig. 8, the maximum adsorption occurred during the first 20 min and then gradually decreased until the formation of an equilibrium state.

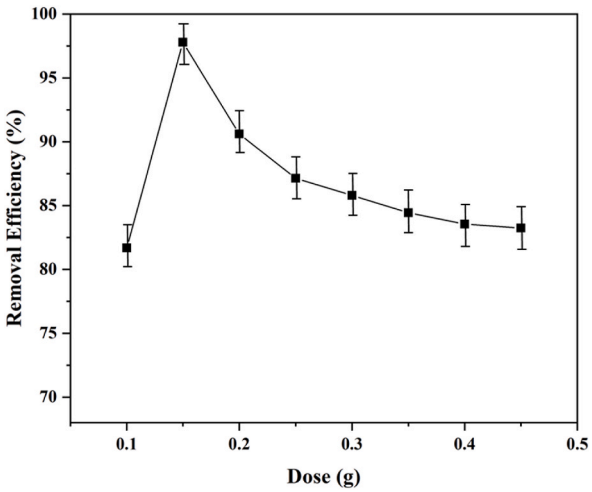

Fig. 6. Effect of adsorbent dose on dye removal.

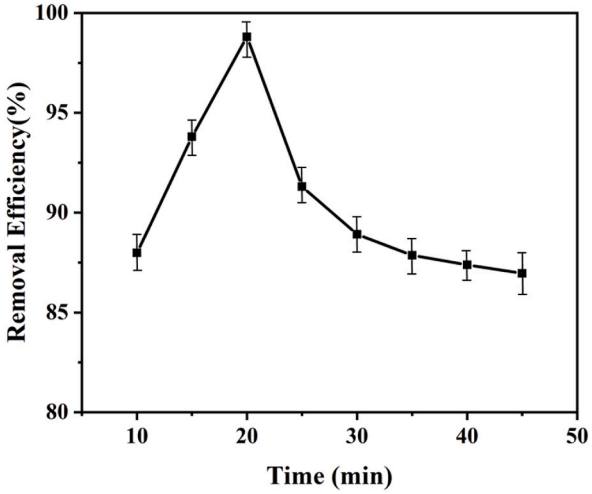

Fig. 7. Effect of contact time on dye removal.

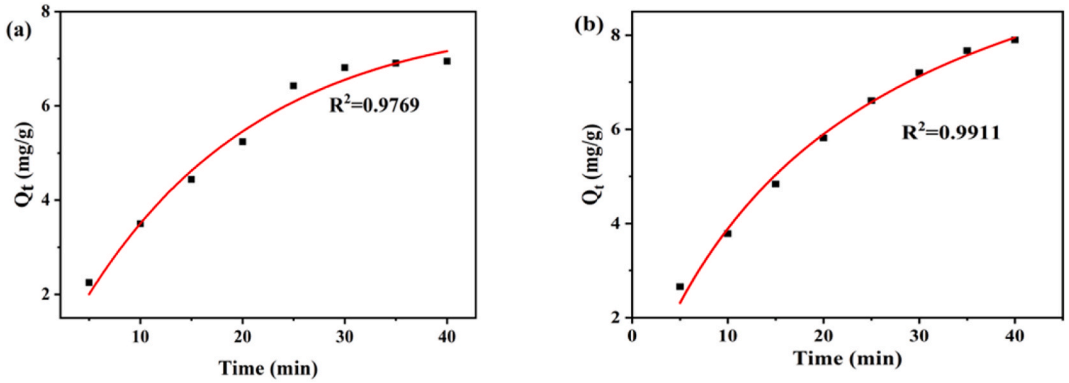

Fig. 8. Non-linear Plot of (a) pseudo-first-order and (b) second-order kinetic model.

3.6. Adsorption kinetics

Mass transfer, diffusion control, and reagent reactions are only a few of the adsorption mechanisms that are significantly influenced by adsorption kinetics. Adsorption occurred in three steps, including adsorbate migration onto the adsorbent surface, adsorbate diffusion up to the boundary layer, and adsorbate diffusion from the surface to the interior of the adsorbent. Most commonly, adsorption rate and type are determined using the pseudo-first-order and pseudo-second order models, respectively. Through the evaluation of coefficient value (R^2), the rationality of the adsorption process is assessed [45].

3.6.1. Pseudo-first-order kinetics

This model was used to examine the adsorption rate of nanocomposites. The following is the equation for pseudo-first-order kinetics:

$$Q_t = Q_e\ (1 - e^{-k1t}) \quad \text{(i)}$$

In this equation, Q_e stands for adsorbate removal at equilibrium (mg/g), whereas Q_t represents adsorbate removal (mg/g) at a certain time and k_1 stands for the absorption rate constant (min^{-1}), respectively. Via the compatibility with such a model, the physisorption of contaminants may be demonstrated [46]. In this kinetics model, the adsorption process is further controlled by the type of the adsorbate.

3.6.2. Pseudo-second-order kinetics

It is well known that the rate-limiting phase in pseudo-second-order kinetics is the electron sharing between adsorbate and adsorbent. The following is the model equation:

$$Q_t = \frac{k_2 Q_e^2 t}{1 + k_2 Q_e t} \quad \text{(ii)}$$

Here, Q_e and Q_t are, respectively, the adsorbed mass per unit mass (mg/g) values of the suspended solids at equilibrium and at a certain period. Similar to k_1, k_2 is the pseudo-second-order operation rate constant (mg/mg/min), which can be affected by a variety of variables including pH, temperature, and the initial concentration of the solution. Based on the adsorption process using the pseudo-second-order model, chemisorption could be recommended [20,47].

Here, pseudo-first-order and pseudo-second-order kinetics models are depicted in Fig. 8(a) and Fig. 8(b), respectively. It has been noted that the second-order kinetics coefficient (R^2) was 0.9911, which is greater than the first-order kinetics coefficient (0.9769). Due to the functional groups that were accessible, it was determined that the adsorption between the dye molecules and the GO-K10 nanocomposites was irreversible and that the adsorption process was mostly chemisorption.

3.7. Adsorption isotherm

Adsorption isotherm is essential to elucidate the interacting behavior between adsorbent and adsorbate in order to evaluate adsorption performance. Three isotherm models, including Langmuir, Freundlich, and Temkin, are commonly investigated in adsorption studies with this goal in mind. The coefficient value of isotherms may be used to estimate the fitness with any of these models (R^2).

3.7.1. Langmuir isotherm

The following is the non-linear equation for the Langmuir isotherm model:

$$Q_e = \frac{Q_m b C_e}{1 + b C_e} \quad \text{(iii)}$$

Where, Q_e represents the equilibrium quantity of adsorbed suspended particles (mg/g), C_e represents the equilibrium concentration of the solution (mg/L), b represents the adsorption equilibrium constant (L/mg) linked to the adsorption energy, and Q_m represents the maximum adsorption capacity. The homogeneous/uniform nature of the accessible adsorbent surface was validated by this model, which denotes monolayer adsorption [20,48,49].

3.7.2. Freundlich isotherm

The following is the non-linear equation for the Freundlich isotherm model:

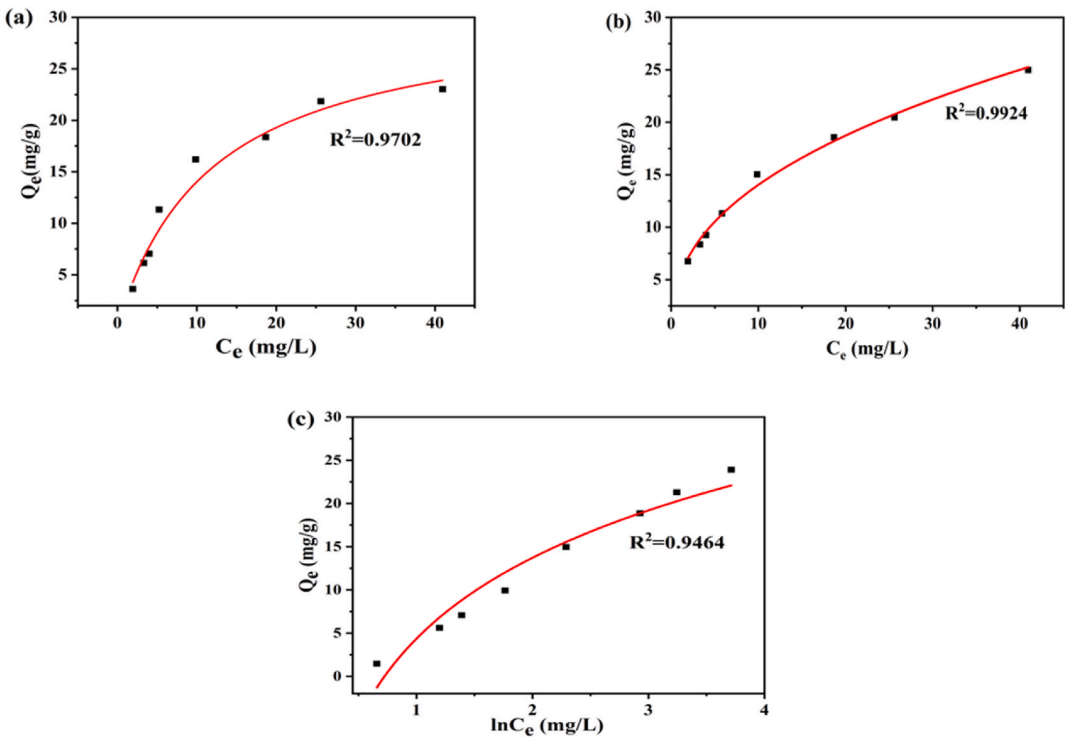

Fig. 9. Non-linear Plot of (a) Langmuir isotherm, (b) Freundlich isotherm and (c) Temkin isotherm.

$$Q_e = K_F C_e^{1/n} \quad \text{(iv)}$$

Here, Qe and Ce are the equilibrium substrate concentration (mg/L) and the amount of adsorbed suspended solids (mg/g), respectively. The Freundlich constants KF and n, which reflect the heterogeneity factor and the adsorption capacity, respectively, are used in the equation. This isotherm model and proven multilayer surface adsorption may describe how the adsorbent interacts with the heterogeneous active binding sites [50].

3.7.3. Isotherm of Temkin model

Temkin isotherm model is thought to be a significant tool for determining the adsorbent-adsorbate surface interaction [51]. The following is the non-linear equation for the Temkin isotherm model:

$$Q_e = \frac{R_T}{b} \ln(A_T C_e) \quad \text{(v)}$$

$$Q_e = \frac{R_T}{b} \ln A_T + \frac{R_T}{b} \ln C_e$$

$$Q_e = B \ln A_T + B \ln C_e \quad \text{(vi)}$$

Here, Ce stands for the equilibrium concentration of the adsorbate (suspended solid), Qe for the amount of adsorbate adsorbed at equilibrium, B = RT/b for the adsorption heat constant, R for the universal gas constant (8.314 J/mol K), T for the temperature in Kelvin (K), b for the Temkin isotherm constant (J/mg) to verify the adsorption energy at equilibrium, and AT for the binding constant, that accordingly, corresponds to the highest binding energy (L/mg).

Fig. 9 depicts the correlation coefficient value of isotherms (R^2) in accordance with the experimental results. Langmuir, Freundlich, and Temkin isotherms had correlation coefficient values (R^2) of 0.9702, 0.9924, and 0.9464, respectively. Nevertheless, it's worth noting that the maximum adsorption capacity observed in the Langmuir isotherm during our experiments was 23.02 mg/g. In recent research, GO-based nanocomposite adsorbents have been employed for wastewater turbidity removal, demonstrating an adsorption capacity of 67.7 mg/g [19]. Therefore, the adsorption mechanism mostly followed the Freundlich isotherm with adsorption capacity of 24.99 mg/g, so it can be anticipated that multilayer adsorption took place into the active sites of GO-K10 nanocomposite to combat anionic dye molecules. The adsorption mechanism of GO-K10 nanocomposite is shown in Fig. 10.

3.8. Wastewater parameters (before and after)

Following a comprehensive analysis, the experimental parameters were meticulously compared and are detailed in Table 2. Notably, our study achieved an impressive 98.8 % turbidity removal, marking a significant milestone in the realm of wastewater treatment. Furthermore, the levels of Biological Oxygen Demand (BOD) and Chemical Oxygen Demand (COD) exhibited substantial reductions of 62 % and 79 %, respectively, underscoring the effectiveness of our approach in mitigating pollutant concentrations. It's worth mentioning that the slight increase in conductivity can be attributed to the inherently conductive nature of the GO-based nanocomposite, a phenomenon that aligns with the findings of a recent study [52].

3.9. Comparison of dye adsorption performance with previous studies

Table 3 underscores a significant research gap in the removal of dye from real tannery wastewater using bio-based nanocomposites, which this study admirably addresses with novelty. Traditional adsorbents have shown limited efficacy in dye removal from tannery effluent, often achieving only marginal results. In many adsorption studies, reliance has been placed on synthetic effluents, neglecting the complexity of real effluent. This oversight can result in unreliable outcomes when optimizing procedures for industrial wastewater treatment [20,21,53,54]. While single-component studies are valuable for understanding the process's mechanics, they may not be as practical for industrial applications. Notably, the synergistic combination of keratin and GO in the GO-K10 composite achieved an impressive 98.8 % turbid dye removal efficiency in tannery wastewater, surpassing other bio-based treatments. Better dye removal performance as an adsorbent was demonstrated by the GO-K10 nanocomposite compared to the previous studies [22,54–60]. The composite's performance is intricately influenced by factors such as the matrix-fiber ratio, fabrication techniques, compatibility between matrix and fiber, fiber length, and the type of materials used [61–65]. This nanocomposite offers standout solution for sustainable leather dyeing effluent treatment. The unique amalgamation of keratin and GO not only focuses on waste management and composite fabrication but also minimizes re-aggregation tendencies and surface area loss, further solidifying the experiment's exceptional significance in the field of dye removal from leather dyeing effluent [64].

4. Conclusion

Keratin in combination with GO was successfully utilized to fabricate the GO-K nanocomposite for removing dye from tannery wastewater. A comprehensive analysis using FTIR, SEM, XRD, and UV–visible spectroscopy (UV–visible spectrum) was carried out to evaluate the successful fabrication of the nanocomposite. The outstanding dispersibility, the existence of amide linkages between GO-K, the crystallinity, and the functionality of the fabricated nanocomposite were confirmed by these analytical methods. Remarkably,

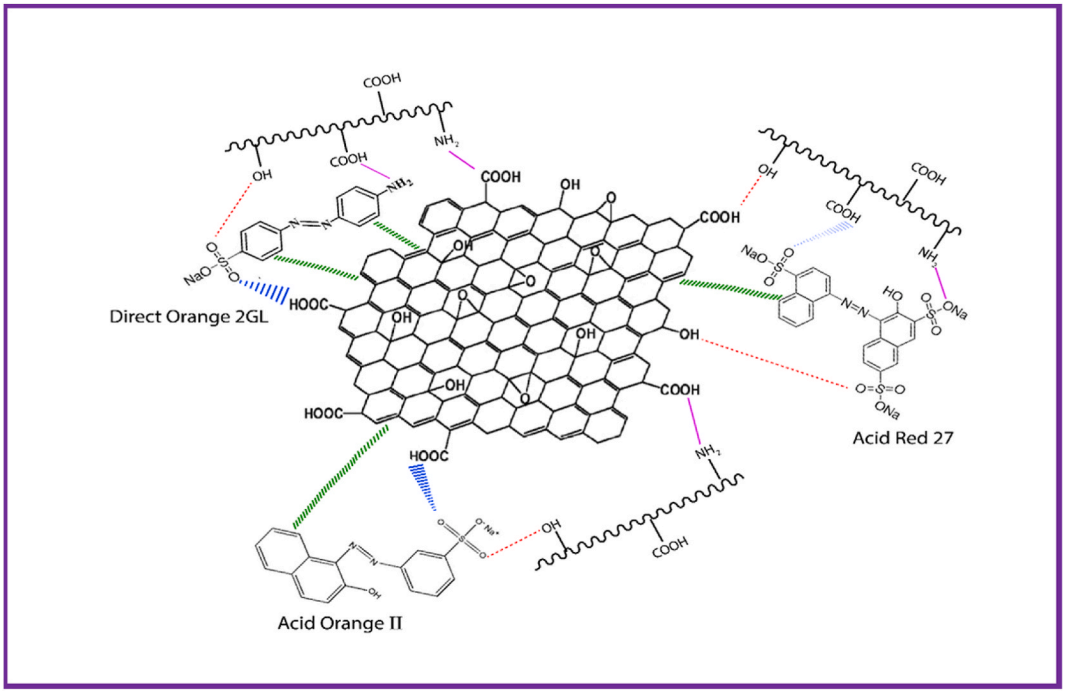

Fig. 10. Adsorption mechanism of GO-K10 nanocomposite with the dyes.

Table 2
Comparison of different parameters between before and after treatment.

Parameters	Raw Effluents	Treated effluent	Standard Value (ECR 97)
pH	3.8	5	3–9
Turbidity	0.531	0.017	–
DO (mg/L)	2.76	5.82	4–6
BOD (mg/L)	1768.52	676.34	100
COD (mg/L)	7012.59	1472.71	400

Table 3
Comparison of dye adsorption performance of various studies.

Treatment Technology	Type of solution	Applied materials	Removal percentage %	References
Adsorption	Leather dyeing wastewater	Graphene Oxide-Keratin nanocomposite	98.8	This Study
Adsorption	Reactive black 5 dye	Keratin based adsorbent	95.3	[22]
Adsorption	Reactive brilliant blue KN-R dye	Keratin composite film	98.52	[55]
Adsorption	Synthetic Azo Dye	Graphene oxide nanoplatelets	97.78 %	[54]
Adsorption	Acid Blue 161 dye	Tannery cattle hair waste	70.82	[56]
Adsorption	Post tanning effluent	Keratin-Polysulfone Blend Membranes	76	[57]
Adsorption	Tannery effluent with cationic dyes	Graphene Oxide	91.2	[58]
Adsorption	Methylene Blue dye	GO-SiO_2-AR	95.08	[59]
Adsorption	Textile wastewater	Graphene oxide	90	[60]
Adsorption	Acid red 27	Polypyrrole/SrFe12O12/Graphene Oxide	99 %	[66]
Adsorption	Methylene Blue	Graphene Oxide	99 %	[67]

when applied at a pH of 5 with an adsorbent dose of 1.5 gL^{-1} over a 20-min contact period, the nanocomposite achieved an exceptional (98.8 %) reduction in dyes. This outcome further affirmed the robust physico-chemical interaction between the adsorbate and the adsorbent. Moreover, the study revealed that pH, contact time, and optimal dosage significantly influenced preventing adsorbent precipitation or aggregation, ensuring the attainment of equilibrium within the designated reaction time. Additionally, the GO-K nanocomposite demonstrated a substantial reduction in both Biological Oxygen Demand (BOD) and Chemical Oxygen Demand (COD) by 62 % and 79 %, respectively. The results indicated not only the ability of GO-K10 nanocomposite to efficiently eliminate

turbid dye but also other important factors, making it a viable option for treating leather dyeing wastewater. However, further investigations should investigate its degradation, desorption characteristics, and reusability to ensure its industrial viability.

Data availability statement

The data are not publicly available due to privacy or ethnic restrictions. The datasets used and/or analyzed during this study are available from the corresponding author on reasonable request.

Ethics approval

Not applicable.

Consent to participate

Not applicable.

Funding statement

Not applicable.

CRediT authorship contribution statement

Shazneen Chowdhury: Methodology. **Md Elias Uddin:** Supervision. **Md Ashikur Rahaman Noyon:** Formal analysis, Data curation. **Md Mahmudul Hassan Mondol:** Writing - review & editing, Visualization. **Ibrahim M. Maafa:** Writing - review & editing. **Ayman Yousef:** Writing - review & editing.

Declaration of competing interest

The authors declare the following financial interests/personal relationships which may be considered as potential competing interests:Dr. Md. Elias Uddin reports was provided by Khulna University of Engineering and Technology. Dr. Md. Elias Uddin reports a relationship with Khulna University of Engineering and Technology that includes: employment.

Acknowledgments

The author extends his appreciation to the Deputyship for Research & Innovation, Ministry of Education in Saudi Arabia for funding this research work through the project number ISP23-58. This study was also supported by Research and Extension (R&E), Khulna University of Engineering & Technology, Khulna, Bangladesh (2023–2024).

Appendix A. Supplementary data

Supplementary data to this article can be found online at https://doi.org/10.1016/j.heliyon.2023.e23421.

References

[1] F. Aeenjan, V. Javanbakht, Methylene blue removal from aqueous solution by magnetic clinoptilolite/chitosan/EDTA nanocomposite, Res. Chem. Intermed. 44 (2017) 1459–1483, https://doi.org/10.1007/s11164-017-3179-x.
[2] S. Afroze, T.K. Sen, A review on heavy metal ions and dye adsorption from water by agricultural solid waste adsorbents, Water Air Soil Pollut. 229 (2018) 1–50, https://doi.org/10.1007/s11270-018-3869-z.
[3] M.A. Juel, M.A. Noyon, A. Mizan, M.A. Hashem, M.G. Azam, Phytoextraction of heavy metals from tannery sludge: a cleaner approach, Environ. Prog. Sustain. Energy 41 (6) (2022), e13928, https://doi.org/10.1002/ep.13928.
[4] P. Mahajan, J. Kaushal, A. Upmanyu, J. Bhatti, Assessment of phytoremediation potential of chara vulgaris to treat toxic pollutants of textile effluent, 2019, J. Toxicol. (2019) 1–11, https://doi.org/10.1155/2019/8351272.
[5] J.S. Piccin, C.S. Gomes, B. Mella, M. Gutterres, Color removal from real leather dyeing effluent using tannery waste as an adsorbent, J. Environ. Chem. Eng. 4 (1) (2016) 1061–1067, https://doi.org/10.1016/j.jece.2016.01.010.
[6] M.C. Kannaujiya, R. Kumar, T. Mandal, M.K. Mondal, Experimental investigations of hazardous leather industry dye (Acid Yellow 2GL) removal from simulated wastewater using a promising integrated approach, Process Saf. Environ. Protect. 155 (2021) 444–454, https://doi.org/10.1016/j.psep.2021.09.040.
[7] S. Khan, A. Malik, Environmental and health effects of textile industry wastewater, in: A. Malik, E. Grohmann, R. Akhtar (Eds.), Environmental Deterioration and Human Health, Natural and Anthropogenic Determinants, 2014, pp. 55–71, https://doi.org/10.1007/978-94-007-7890-0_4.
[8] M. Solak, M. Kılıç, Y. Hüseyin, A. Şencan, Removal of suspended solids and turbidity from marble processing wastewaters by electrocoagulation: Comparison of electrode materials and electrode connection systems, J. Hazard Mater. 172 (2009) 345–352, https://doi.org/10.1016/j.jhazmat.2009.07.018.
[9] Desta MB (2013) batch sorption experiments: Langmuir and Freundlich isotherm studies for the adsorption of textile metal ions onto teff straw (eragrostis tef) agricultural waste, J Thermodyn (2013) 1–6, https://doi.org/10.1155/2013/375830.

[10] K.O. Iwuozor, Prospects and challenges of using coagulation-flocculation method in the treatment of effluents, Adv J Chem-Section A 2 (2) (2019) 105–127, https://doi.org/10.29088/SAMI/AJCA.2019.2.105127.

[11] B. Yu, Y. Bai, Z. Ming, H. Yang, L. Chen, X. Hu, S. Feng, S.T. Yang, Adsorption behaviors of tetracycline on magnetic graphene oxide sponge, Mater. Chem. Phys. 198 (2017) 283–290, https://doi.org/10.1016/j.matchemphys.2017.05.042.

[12] Al-Khaldi FA. Ihsanullah, B. Abu-Sharkh, A.M. Abulkibash, M.I. Qureshi, T. Laoui, M.A. Atieh, Effect of acid modification on adsorption of hexavalent chromium (Cr (VI)) from aqueous solution by activated carbon and carbon nanotubes, Desalination Water Treat. 57 (16) (2016) 7232–7244, https://doi.org/10.1080/19443994.2015.1021847.

[13] A.E. Burakov, E.V. Galunin, I.V. Burakova, A.E. Kucherova, S. Agarwal, A.G. Tkachev, V.K. Gupta, Adsorption of heavy metals on conventional and nanostructured materials for wastewater treatment purposes: a review, Ecotoxicol. Environ. Saf. 148 (2018) 702–712, https://doi.org/10.1016/j.ecoenv.2017.11.034.

[14] W. Gao, The Chemistry of Graphene Oxide. Graphene Oxide: Reduction Recipes, Spectroscopy, and Applications, Springer, 2015, https://doi.org/10.1007/978-3-319-15500-5, 61-95.

[15] D. Gaber, M. Abu Haija, A. Eskhan, F. Banat, Graphene as an efficient and reusable adsorbent compared to activated carbons for the removal of phenol from aqueous solutions, Water Air Soil Pollut. 228 (2017) 1–4, https://doi.org/10.1007/s11270-017-3499-x.

[16] M.L. Ramos, G. Galaburri, J.A. González, C.J. Pérez, M.E. Villanueva, G.J. Copello, Influence of GO reinforcement on keratin based smart hydrogel and its application for emerging pollutants removal, J. Environ. Chem. Eng. 6 (6) (2018) 7021–7028, https://doi.org/10.1016/j.jece.2018.11.011.

[17] A.E. Aboubaraka, E.F. Aboelfetoh, E.Z. Ebeid, Coagulation effectiveness of graphene oxide for the removal of turbidity from raw surface water, Chemosphere 181 (2017) 738–746, https://doi.org/10.1016/j.chemosphere.2017.04.137.

[18] C.M. Bezerra de Araujo, G. Filipe Oliveira do Nascimento, G. Rodrigues Bezerra da Costa, K. Santos da Silva, A.M. Salgueiro Baptisttella, M. Gomes Ghislandi, M. Alves da Motta Sobrinho, Adsorptive removal of dye from real textile wastewater using graphene oxide produced via modifications of hummers method, Chem. Eng. Commun. 206 (2018) 1375–1387, https://doi.org/10.1080/00986445.2018.1534232.

[19] K. Roy, T.K. Dey, S.T. Zuha, M. Jamal, M. Srivastava, M.E. Uddin, Removal of turbidity from tannery wastewater using graphene oxide-ferric oxide nanocomposites as an adsorbent, Int. J. Environ. Sci. Technol. 20 (5) (2022) 5597–5608, https://doi.org/10.1007/s13762-022-04301-w.

[20] K. Roy, T.K. Dey, M. Jamal, R. Rathanasamy, M. Chinnasamy, M.E. Uddin, Fabrication of graphene oxide–keratin–chitosan nanocomposite as an adsorbent to remove turbidity from tannery wastewater Water, Sci Eng 16 (2) (2023) 184–191, https://doi.org/10.1016/j.wse.2022.12.003.

[21] R. Pankaj, K. Jyoti, S. Pooja, S. Pardeep, Kinetics of photocatalytic mineralization of oxytetracycline and ampicillin using activated carbon supported ZnO/ZnWO4 nanocomposite in simulated wastewater, Desalination Water Treat. 79 (2017) 204–213, https://doi.org/10.5004/dwt.2017.20831.

[22] W. Zhu, X. Qian, H. Yu, X. Li, K. Song, Fabrication of mechanical robust keratin adsorbent by induced molecular network transition and its dye adsorption performance, Environ. Sci. Pollut. Res. 27 (33) (2020) 41577–41584, https://doi.org/10.1007/s11356-020-10165-9.

[23] A. Aluigi, C. Vineis, C. Tonin, C. Tonetti, A. Varesano, G. Mazzuchetti, Wool keratin-based nanofibres for active filtration of air and water, J. Biobased Mater. Bioenergy 3 (2009) 311–319, https://doi.org/10.1166/jbmb.2009.1039.

[24] B. Wang, W. Yang, J. McKittrick, M.A. Meyers, Keratin: structure, mechanical properties, occurrence in biological organisms, and efforts at bioinspiration, Prog. Mater. Sci. 76 (2016) 229–318, https://doi.org/10.1016/j.pmatsci.2015.06.001.

[25] A. Kheradmand, M. Negarestani, S. Kazemi, H. Shayesteh, S. Javanshir, H. Ghiasinejad, Adsorption behavior of rhamnolipid modified magnetic Co/Al layered double hydroxide for the removal of cationic and anionic dyes, Sci. Rep. 12 (1) (2022), 14623, https://doi.org/10.1038/s41598-022-19056-0.

[26] R. Al-Tohamy, S.S. Ali, F. Li, K.M. Okasha, Y.A.G. Mahmoud, T. Elsamahy, J. Sun, A critical review on the treatment of dye-containing wastewater: ecotoxicological and health concerns of textile dyes and possible remediation approaches for environmental safety, Ecotoxicol. Environ. Saf. 231 (2022), 113160, https://doi.org/10.1016/j.ecoenv.2021.113160.

[27] M.E. Uddin, T. Kuila, G.C. Nayak, N.H. Kim, B.C. Ku, J.H. Lee, Effects of various surfactants on the dispersion stability and electrical conductivity of surface modified graphene, J. Alloys Compd. 562 (2013) 134–142, https://doi.org/10.1016/j.jallcom.2013.01.127.

[28] J. He, D. Xu, J. Li, L. Li, W. Li, W. Cui, K. Liu, Highly efficient extraction of large molecular-weight keratin from wool in a water/ethanol co-solvent, Textil. Res. J. 90 (9–10) (2020) 1084–1093, https://doi.org/10.1177/0040517519885022.

[29] N. Akter, S. Chakma, K. Fatema, A.K. Azad, M. Jaman Chowdhury, M. Abu Sayid Mia, Alkali enzymatic extraction of keratin protein from chicken feather waste in Bangladesh, Iran. J. Energy Environ. 10 (4) (2019) 235–241, https://doi.org/10.5829/ijee.2019.10.04.02.

[30] T. Tanabe, N. Okitsu, A. Tachibana, K. Yamauchi, Preparation and characterization of keratin-chitosan composite film, Biomater 23 (2002) 817–825, https://doi.org/10.1016/s0142-9612(01)00187-9.

[31] M.E. Uddin, R.K. Layek, H.Y. Kim, N.H. Kim, D. Hui, J.H. Lee, Preparation and enhanced mechanical properties of non-covalently-functionalized graphene oxide/cellulose acetate nanocomposites, Compos. B Eng. 90 (2016) 223–231, https://doi.org/10.1016/j.compositesb.2015.12.008.

[32] X. Yang, C. Chen, J. Li, G. Zhao, X. Ren, X. Wang, Graphene oxide-iron oxide and reduced graphene oxide-iron oxide hybrid materials for the removal of organic and inorganic pollutants, RSC Adv. 2 (23) (2012) 8821–8826, https://doi.org/10.1039/C2RA20885G.

[33] J.P. Cheng, Q.L. Shou, J.S. Wu, F. Liu, V.P. Dravid, X.B. Zhang, Influence of component content on the capacitance of magnetite/reduced graphene oxide composite, J. Electroanal. Chem. 698 (2013) 10–18, https://doi.org/10.1016/j.jelechem.2013.03.017.

[34] C. Sun, Z. Wang, L. Chen, F. Li, Fabrication of robust and compressive chitin and graphene oxide sponges for removal of microplastics with different functional groups, Chem Eng J 393 (2020), 124796, https://doi.org/10.1016/j.cej.2020.124796.

[35] A.N. Kamarudin, K.S. Lai, D.U. Lamasudin, A.S. Idris, Z.N. Balia Yusof, Enhancement of thiamine biosynthesis in oil palm seedlings by colonization of endophytic fungus Hendersonia toruloidea, Front. Plant Sci. 8 (2017) 1799, https://doi.org/10.3389/fpls.2017.01799.

[36] Q. Lai, S. Zhu, X. Luo, M. Zou, S. Huang, Ultraviolet-visible spectroscopy of graphene oxides, AIP Adv. 2 (2012) 3, https://doi.org/10.1063/1.4747817.

[37] P. Shandilya, D. Mittal, M. Soni, P. Raizada, A. Hosseini-Bandegharaei, A.K. Saini, P. Singh, Fabrication of fluorine doped graphene and SmVO4 based dispersed and adsorptive photocatalyst for abatement of phenolic compounds from water and bacterial disinfection, J. Clean. Prod. 203 (2018) 386–399, https://doi.org/10.1016/j.jclepro.2018.08.271.

[38] X. Gong, G. Dang, J. Guo, Y. Liu, Y. Gong, A sodium alginate/feather keratin composite fiber with skin-core structure as the carrier for sustained drug release, Int. J. Biol. Macromol. 155 (2020) 386–392, https://doi.org/10.1016/j.ijbiomac.2020.03.224.

[39] V. Dhayal, S.Z. Hashmi, U. Kumar, B.L. Choudhary, A.E. Kuznetsov, S. Dalela, S. Kumar, S. Kaya, S.N. Dolia, P.A. Alvi, Spectroscopic studies, molecular structure optimization and investigation of structural and electrical properties of novel and biodegradable Chitosan-GO polymer nanocomposites, J. Mater. Sci. 55 (2020) 14829–14834, https://doi.org/10.1007/s10853-020-05093-5.

[40] M. Pooresmaeil, H. Namazi, Application of polysaccharide-based hydrogels for water treatments, in: Hydrogels Based on Natural Polymers, Elsevier, 2020, pp. 411–455, https://doi.org/10.1016/B978-0-12-816421-1.00014-8.

[41] F. Khan, M.S. Khan, S. Kamal, M. Arshad, S.I. Ahmad, S.A.A. Nami, Recent advances in graphene oxide and reduced graphene oxide based nanocomposites for the photodegradation of dyes, J. Mater. Chem. C 8 (2020) 15940–15955, https://doi.org/10.1039/d0tc03684f.

[42] N.N. Rudi, M.S. Muhamad, L. Te Chuan, J. Alipal, S. Omar, N. Hamidon, N.H. Hamid, N.M. Sunar, R. Ali, H. Harun, Evolution of adsorption process for manganese removal in water via agricultural waste adsorbents, Heliyon 6 (9) (2020), e05049, https://doi.org/10.1016/j.heliyon.2020.e05049.

[43] J. Anandkumar, B. Mandal, Removal of Cr(VI) from aqueous solution using Bael fruit (Aegle marmelos correa) shell as an adsorbent, J. Hazard Mater. 168 (2009) 633–640, https://doi.org/10.1016/j.jhazmat.2009.02.136.

[44] V. Soni, P. Singh, S. Thakur, P. Thakur, T. Ahamad, V.H. Nguyen, P. Raizada, Fabricating cattle dung-derived nitrogen-doped biochar supported oxygen-deficient ZnO and Cu2O-based novel step-scheme photocatalytic system for aqueous Doxycycline hydrochloride mitigation and Cr (VI) reduction, J. Environ. Chem. Eng. 11 (5) (2023), 110856, https://doi.org/10.1016/j.jece.2023.110856.

[45] R. Bai, Y. Zhang, Z. Zhao, Q. Liao, P. Chen, P. Zhao, W. Guo, F. Yang, L. Li, Rapid and highly selective removal of lead in simulated wastewater of rare-earth industry using diglycolamic-acid functionalized magnetic chitosan adsorbents, J. Ind. Eng. Chem. 59 (2018) 416–424, https://doi.org/10.1016/j.jiec.2017.10.053.

[46] P. Miralinaghi, P. Kashani, E. Moniri, M. Miralinaghi, Non-linear kinetic, equilibrium, and thermodynamic studies of 5-fluorouracil adsorption onto chitosan–functionalized graphene oxide, Mater. Res. Express 6 (6) (2019), 065305, https://doi.org/10.1088/2053-1591/ab0831.
[47] G.R. Mahdavinia, A. Mosallanezhad, Facile and green rout to prepare magnetic and chitosan-crosslinked κ-carrageenan bionanocomposites for removal of methylene blue, J. Water Proc. Eng. 10 (2016) 143–155, https://doi.org/10.1088/2053-1591/ab0831.
[48] F. Amini Tapouk, R. Nabizadeh, S. Nasseri, A. Mesdaghinia, H. Khorsandi, M. Yousefi, M. Alimohammadi, M. Khoobi, Embedding of L–Arginine into graphene oxide (GO) for endotoxin removal from water: modeling and optimization approach, Colloids Surf. A Physicochem. Eng. Asp. 607 (2020), 125491, https://doi.org/10.1016/j.colsurfa.2020.125491.
[49] M. Yousefi, M. Gholami, V. Oskoei, A.A. Mohammadi, M. Baziar, A. Esrafili, Comparison of LSSVM and RSM in simulating the removal of ciprofloxacin from aqueous solutions using magnetization of functionalized multi-walled carbon nanotubes: process optimization using GA and RSM techniques, J. Environ. Chem. Eng. 9 (4) (2021), 105677, https://doi.org/10.1016/j.jece.2021.105677.
[50] M.K. Amosa, M.S. Jami, M.F.R. Alkhatib, T. Tajari, D.N. Jimat, R.U. Owolabi, Turbidity and suspended solids removal from high-strength wastewater using high surface area adsorbent: mechanistic pathway and statistical analysis, Cogent Eng 3 (1) (2016), 1162384, https://doi.org/10.1080/23311916.2016.1162384.
[51] A. Kausar, F. Sher, A. Hazafa, A. Javed, M. Sillanpää, M. Iqbal, Biocomposite of sodium-alginate with acidified clay for wastewater treatment: kinetic, equilibrium and thermodynamic studies, Int. J. Biol. Macromol. 161 (2020) 1272–1285, https://doi.org/10.1016/j.ijbiomac.2020.05.26.
[52] I. Ali, A.A. Basheer, X.Y. Mbianda, A. Burakov, E. Galunin, I. Burakova, E. Mkrtchyan, A. Tkachev, V. Grachev, Graphene based adsorbents for remediation of noxious pollutants from wastewater, Environ. Int. 127 (2019) 160–180, https://doi.org/10.1016/j.envint.2019.03.029.
[53] J.O. Unuofin, A.I. Okoh, U.U. Nwodo, Aptitude of oxidative enzymes for treatment of wastewater pollutants: a laccase perspective, Molecules 24 (11) (2019) 2064, https://doi.org/10.3390/molecules24112064.
[54] P. Banerjee, S. Sau, P. Das, A. Mukhopadhayay, Optimization and modelling of synthetic azo dye wastewater treatment using Graphene oxide nanoplatelets: characterization toxicity evaluation and optimization using Artificial Neural Network, Ecotoxicol. Environ. Saf. 119 (2015) 47–57, https://doi.org/10.1016/j.ecoenv.2015.04.022.
[55] K. Song, X. Qian, X. Zhu, X. Li, X. Hong, Fabrication of mechanical robust keratin film by mesoscopic molecular network reconstruction and its performance for dye removal, J. Colloid Interface Sci. 579 (2020) 28–36, https://doi.org/10.1016/j.jcis.2020.06.026.
[56] B. Mella, M. Gutterres, Preparation and characterisation of tannery solid waste as an alternative biosorbent for leather dyes, J. Soc. Leather Technol. Chem. 101 (2017) 143.
[57] A. Karunanidhi, P.S. David, N.N. Fathima, Electrospun keratin-polysulfone blend membranes for treatment of tannery effluents, Water Air Soil Pollut. 231 (2020) 1–11, https://doi.org/10.1007/s11270-020-04682-z.
[58] M.I. Hossain, A.K. Deb, M.Z. Sultan, A.A. Shaikh, M. Chowdhury, M.R. Sarker, Synthesis and application of graphene oxide (go) for removal of cationic dyes from tannery effluents, Text leather Rev 3 (3) (2020) 146–157, https://doi.org/10.31881/tlr.2020.12.
[59] K.D. Lokhande, D.A. Pethsangave, D.K. Kulal, S. Some, Remediation of toxic dye pollutants by using graphene-based adsorbents, ChemistrySelect 5 (2020) 8062–8073, https://doi.org/10.1002/slct.202002130.
[60] C.M.B. Araújo, G.F. Oliveira do Nascimento, G.R. Bezerra da Costa, A.M.S. Baptisttella, T.J.M. Fraga, R.B. Assis Filho, M.G. Ghislandi, M.A. Motta Sobrinho, Real textile wastewater treatment using nano graphene-based materials: optimum pH, dosage, and kinetics for colour and turbidity removal, Can. J. Chem. Eng. 98 (2020) 1429–1440, https://doi.org/10.1002/cjce.23712.
[61] M.A. Noyon, T.K. Dey, M. Jamal, R. Rathanasamy, M. Chinnasamy, M.E. Uddin, Fabrication of LLDPE based biodegradable composite incorporated with leather shavings and buffing dust: an approach for waste management, J. Appl. Polym. Sci. 139 (47) (2022), e53184, https://doi.org/10.1002/app.53184.
[62] H. Ahmed, M.A.R. Noyon, M.E. Uddin, M. Jamal, S.K. Palaniappan, Biodegradable and flexible fiber-reinforced composite sheet from tannery solid wastes: an approach of waste minimization, Polym. Compos. 2023 (2023) 1–12, https://doi.org/10.1002/pc.27644.
[63] M.A.R. Noyon, M.S. Karim, M.A. Rouf, M. Jamal, R.K. Layek, G. Sivanantham, M.E. Uddin, Fabrication of biodegradable kraft paper from buffing dust and jute fiber: green solutions for packaging, Polym. Eng. Sci. (2023) 1–11, https://doi.org/10.1002/pen.26503.
[64] R. Islam, M.A.R. Noyon, T.K. Dey, M. Jamal, R. Rathanasamy, M. Chinnasamy, M.E. Uddin, Fabrication of graphene oxide reinforced biocomposite: recycling of postconsumed footwear leather, Adv. Polym. Technol. 2023 (2023) 1–10, https://doi.org/10.1155/2023/3996687.
[65] M.A.R. Noyon, M.E. Uddin, T.K. Dey, M. Jamal, G. Sivanantham, R. Islam, Biodegradable composite from discarded hair keratin and graphene oxide with improved mechanical, thermal and barrier properties: an eco-friendly solution to waste materials, Polym. Int. 2023 (2023) 1–12, https://doi.org/10.1002/pi.6586.
[66] S. Ebrahimpoor, V. Kiarostami, M. Khosravi, M. Davallo, A. Ghaedi, Bees metaheuristic algorithm with the aid of artificial neural networks for optimization of acid red 27 dye adsorption onto novel polypyrrole/SrFe 12 O 19/graphene oxide nanocomposite, Polym. Bull. 76 (2019) 6529–6553, https://doi.org/10.1007/s00289-019-02700-7.
[67] S.T. Yang, S. Chen, Y. Chang, A. Cao, Y. Liu, H. Wang, Removal of methylene blue from aqueous solution by graphene oxide, J. Colloid Interface Sci. 359 (1) (2011) 24–29, https://doi.org/10.1016/j.jcis.2011.02.064.